Building and Environment 223 (2022) 109504

Contents lists available at ScienceDirect

Building and Environment

journal homepage: www.elsevier.com/locate/buildenv

Towards wearable thermal comfort assessment framework by analysis of heart rate variability☆

Ziyang Wang *, Ryuji Matsuhashi, Hiroshi Onodera

Department of Electrical Engineering and Information Systems, The University of Tokyo, Tokyo, 113-8656, Bunkyo, Japan

ARTICLE INFO

Keywords:
Heartbeat sensor
Physiological index
Energy conservation
Fast Fourier Transform
Hilbert transform
Machine learning

ABSTRACT

Buildings consume huge amounts of energy and utilize most of it for occupants' thermal comfort satisfaction. Real-time thermal comfort assessment can enormously contribute to thermal comfort optimization and energy conservation in buildings. Existing thermal comfort models mainly utilize classification algorithms to identify personal thermal comfort states, resulting in significant information loss. In addition, existing thermal comfort studies mainly use the Fast Fourier Transform (FFT) for frequency-domain heart rate variability (HRV) feature extraction to compute the power of the Low-frequency (LF) and High-frequency (HF) bands of the R–R intervals (RRIs), resulting in the insufficient use of the information in the RRIs. To account for these concerns, this study defines personal thermal sensation as a continuous function of time, and investigates using the Hilbert Transform (HT) to extract the instantaneous amplitude (iA) of the LF and HF for thermal comfort modeling. Moreover, a novel continuous thermal sensation acquisition system has been designed to obtain the subjects' approximate continuous thermal sensation. The FFT-based HRV features, HT-based HRV features, and time-domain HRV features have all been shown to be relevant for personal thermal comfort modeling. By utilizing machine learning regressions, it is feasible to combine the HT-based HRV features and other HRV features together to boost personal thermal comfort prediction accuracy. The subjects' personal thermal comfort prediction reached the highest average coefficient of determination (R^2) of 0.73 by using all the HRV features together. This study facilitates practical applications for wearable thermal comfort assessment frameworks and contributes to energy conservation in buildings.

1. Introduction

Buildings consume over one-third of global final energy consumption [1] and use more than 50% of it for the occupants' thermal comfort maintenance through the Heating, Ventilation, and Air Conditioning (HVAC) systems [2]. Accurate real-time thermal comfort assessment is essential and critical in thermal comfort satisfaction, intelligent HVAC system control, and energy conservation in the building sector. Thermal comfort is defined as "the condition of mind that expresses satisfaction with the thermal environment and is assessed by subjective evaluation" [3] by the American Society of Heating, Refrigerating and Air-Conditioning Engineers (ASHRAE) in the ASHRAE Standard 55, indicating that thermal comfort is only determined by one's subjective judgment about the surrounding thermal environment. Thermal comfort studies focused on collective thermal comfort satisfaction in multi-occupancy scenarios have been extensively researched, such as in Jung et al. [4]. In this paper, we investigate personalized thermal comfort assessment in single-occupancy scenarios. Although survey-based methods can make direct extraction of occupants' personal real-time thermal comfort through questionnaires, such as the thermal sensation vote (TSV), continuous feedback provided by the occupants is required.

In single-occupancy scenarios, in order to enhance intelligent HVAC system control, it is necessary to understand the degree of one's thermal comfort as feedback to the control algorithm of the HVAC system. As existing thermal comfort studies usually use classification algorithms to identify discrete personal thermal comfort state (e.g., "uncomfortably hot", "comfortable", or "uncomfortably cold"), many fine details of the real-time thermal sensation will be lost, which impairs the precision of the control algorithm of the HVAC system. For instance, an "uncomfortably hot" state may vary significantly from "slightly hot" to "extremely hot". If the real-time thermal sensation is in a continuous form, the problem can be completely solved.

Due to the fact that individual differences in personal thermal comfort could be reflected in physiological indices, physiological indices should be taken into account. In order to achieve real-time personal

☆ This work was supported in part by the Center of Innovation Stream of the Japan Science and Technology Agency.
* Corresponding author.
E-mail address: wangziyang@g.ecc.u-tokyo.ac.jp (Z. Wang).

https://doi.org/10.1016/j.buildenv.2022.109504
Received 8 June 2022; Received in revised form 26 July 2022; Accepted 13 August 2022
Available online 19 August 2022

Nomenclature

Abbreviations

ASHRAE	American Society of Heating, Refrigerating and Air-conditioning Engineers
HVAC	Heating, Ventilation and Air Conditioning
PMV	Predicted Mean Vote
TSV	Thermal sensation vote
ROI	Region of interest
EEG	Electroencephalogram
RTS	Relative Thermal Sensation
ATS	Absolute Thermal Sensation
7-point ATSS	7-point Absolute Thermal Sensation Scale
ATSV	Absolute Thermal Sensation Vote
ECG	Electrocardiogram
MAP	Mean arterial blood pressure
mPMV	Modified PMV model
HRV	Heart rate variability
RRI	R–R interval
PNS	Parasympathetic nervous system
SNS	Sympathetic nervous system
LF	Low-frequency band (0.04–0.15 Hz)
HF	High-frequency band (0.15–0.4 Hz)
IHR	Instantaneous heart rate
DFT	Discrete Fourier Transform
SDSD	Standard deviation of successive RRIs
RMSSD	Square root of the mean of the sum of the squares of differences between successive RRIs
pNN_{50}	Proportion of the number of RRI differences of successive RRIs which are greater than 50 ms, divided by the total number of RRIs
FFT	Fast Fourier Transform
PSD	Power spectral density
LF_p	Power of the LF
HF_p	Power of the HF
HT	Hilbert Transform
iA	Instantaneous amplitude
LF_{iA}	iA of the LF
HF_{iA}	iA of the HF
Base	Time-domain HRV features
F	FFT features
H	HT features
BaseF	Base and FFT features
BaseH	Base and HT features
FH	FFT and HT features
BaseFH	Base, FFT, and HT features
MLP	Multilayer Perceptron
MSE	Mean squared error
R^2	Coefficient of determination

Symbols

F	Fourier Transform operator
U	Unit step function
μ	Mean value
σ	Standard deviation

Variables

$f(t)$	Continuous thermal comfort at time t
RR_i	ith RRI in successive RRIs
N	Length of a sequence
$x[n]$	Sequence with a length N
$y[k]$	FFT of $x[n]$
$x(t)$	Signal at time t
$x_a(t)$	Analytic signal of $x(t)$
$x_{iA}(t)$	iA of $x_a(t)$
X_t	A certain HRV feature at time t
$\overline{X_t}$	A certain smoothed HRV feature at time t
T_I	Air temperature of the inner chamber (°C)
T_E	Air temperature of the external environment (°C)

thermal comfort assessment using physiological indices and improve comfort, the measurement should neither be cumbersome nor disturbing. With the above-mentioned concerns, the heart rate variability (HRV), which is generally considered to be related to sympathovagal balance [5–7], has drawn attention to thermal comfort modeling in recent years [8–10], which is easy to measure since the heartbeat measurement only requires one portable and non-intrusive heartbeat sensor.

Fig. 1 shows a schematic of an Electrocardiogram (ECG) graph. In the ECG graph, the most prominent wave is called the R wave, as illustrated in Fig. 1. The difference in time between two consecutive R waves is called the R–R interval (RRI). It has been revealed that the RRI generates much more information than the original ECG for stress analysis. The HRV is precisely defined as the physiological phenomenon of the variation in consecutive RRIs. The more variations, the higher the HRV; the fewer the variations, the lower the HRV, as illustrated in the upper and lower parts in Fig. 1.

To address these challenges, in this paper as well as in our previous works [11,12], we define personal thermal sensation to be a continuous function $f(t)$ of time t, where $f(t) > 0$ denotes hot sensation, $f(t) < 0$ denotes cold sensation, $f(t) = 0$ denotes neutral thermal sensation. The larger its absolute value $|f(t)|$, the greater the degree of hotness or coldness. In Wang et al. [11], we proposed the concept of Relative Thermal Sensation (RTS), which is precisely defined as the gradient of the thermal sensation ($f'(t)$), and redefined the thermal sensation in the common sense ($f(t)$) as the Absolute Thermal Sensation (ATS). Then we conducted an experiment to create transient thermal environments and investigate the subject's ATS and RTS assessment methods under such thermal conditions by analysis of the subjects' local body part temperatures measured by thermocouple thermometers. Actually, in Wang et al. [11], we also measured the subjects' RRIs (unit: ms) in real-time through a portable, non-intrusive, and low-cost heartbeat sensor myBeat WHS-1 [13]. In this paper, we investigate using HRV analysis for personal ATS modeling using the subjects' RRIs measured in Wang et al. [11]. The RTS proposed in Wang et al. [11] is beyond the scope of this paper.

The contributions of this paper are illustrated as follows. A novel thermal sensation acquisition system allowing voting at any time has been designed to obtain the subjects' real-time approximate continuous thermal sensation. The proposed thermal comfort learning framework by analysis of HRV indices has been verified to be applicable under transient thermal environments. Frequency-domain HRV features extracted by the Hilbert Transform (HT) have been verified relevant for thermal comfort modeling. By combining the HT-based HRV features and other HRV features together, personal thermal comfort prediction accuracy can be boosted. The paper is organized as follows. The related works are discussed in Section 2. The HRV feature extraction and data analysis method are presented in Section 3. Section 4 illustrates the details of the experimental thermal conditions and data collection procedures. Section 5 shows the results and the performance metrics. Finally, Section 6 concludes the paper.

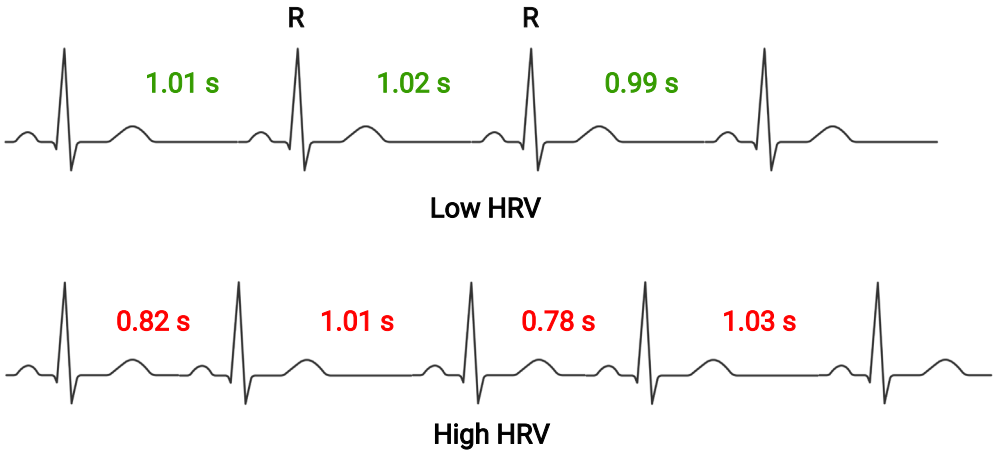

Fig. 1. An illustration of the Heart rate variability (HRV).

2. Related works

This section discusses some representative works on personal thermal comfort assessment by various physiological indices and their drawbacks. It has been revealed that the human thermoregulation system adjusts heat exchange with the surroundings by vasoconstriction and vasodilation of cutaneous vessels in regard to thermal stress (namely, heat or cold) [14,15]. Existing studies have extensively investigated using skin/clothing temperatures or radiation for thermal comfort modeling [16,17]. However, the drawbacks of these skin/clothing temperatures or radiation-based methods are summarized as follows: (1) these methods usually require multiple temperature sensors, decreasing the user experience and comfort; (2) the users have to show desired gestures or deliberate directions to the infrared camera, resulting in an inexpedient manner to assess the users' thermal comfort in some specific scenarios (e.g., (a) sleeping state when the body is covered by the bed quilt; (b) when the user changes the body direction); (3) in order to obtain the users' thermal images omnidirectionally for Region of Interest (ROI) extraction, multiple infrared cameras are required, increasing the apparatus cost; (4) the infrared camera-based method is not applicable in the outdoor environment for wearable cooler users. Yao et al. and Yang et al. [18,19] demonstrated that the electroencephalogram (EEG) could be used for thermal comfort modeling. However, the cumbersome measurement apparatus and the low sensitivity problems remain. In Schmidt et al. [20,21], the authors revealed that cooling as a thermal stimulus during driving can cause an increase in the pupil diameter, indicating that the pupil diameter can serve as a biomarker to thermal stimuli. However, due to the fact that the pupil diameter is affected by substantial factors such as the light and the necessity of using a camera to take a measurement, it is considered not suitable for convenient thermal comfort assessment. Moreover, it has been revealed that with the body exposure to decreasing ambient air temperature, an increase in systolic blood pressure can be caused [22–24]. Gilani et al. [25] demonstrated that the mean blood pressure has a strong correlation with the activity level, and proposed a modified PMV model (mPMV) using mean arterial blood pressure (MAP) instead of activity level. However, some studies indicate that the blood pressure is indefinite to thermal stimulus [26]. Also, real-time blood pressure measurement is expensive and thus considered inappropriate to be applied for convenient thermal comfort measurement.

Compared to multi-point measurement of body surface temperatures, the heartbeat measurement is much easier to achieve since it only requires one portable and non-intrusive heartbeat sensor even though in extreme conditions when the occupant's body is covered by the bed quilt during sleeping state. Suppose the HRV can represent personal thermal comfort. In that case, it could be promising for the implementation of a convenient and wearable thermal comfort assessment framework using such a portable and non-intrusive heartbeat sensor, which is not only applicable in the indoor environment but also in the outdoor environment for wearable cooler users.

Preceding studies have shown that power spectrum analysis of the HRV can provide a quantitative non-intrusive method for assessing the sympathovagal balance [27–29]. The activities of the sympathetic nervous system (SNS) and parasympathetic nervous system (PNS) contribute to the heart rate power spectrum at specific frequencies. Fig. 2 shows a schematic of the heart rate power spectrum. Substantial empirical evidence has shown that the activity of the SNS has an impact on the Low-frequency band (LF) of the heart rate power spectrum, from 0.04–0.15 Hz, whilst the PNS influences the High-frequency band (HF) of the heart rate power spectrum, from 0.15–0.4 Hz, and also probably a proportion of the LF [30–33]. In order to distinguish from the frequency bands, we adopt a subscript "p" in a frequency band to denote its power (LF_p and HF_p). The LF_p, HF_p, and LF_p/HF_p have been adopted as stress biomarkers in substantial studies [5,34–36]. Liu et al. [8] revealed that the LF_p/HF_p at comfort level was significantly lower than that at discomfort level ($P < 0.05$) and demonstrated that the LF_p/HF_p could be used for thermal comfort modeling. Morresi et al. [37–39] conducted a series of studies to investigate the feasibility of using HRV indices for personal thermal comfort modeling, and demonstrated that only using LF_p/HF_p to predict personal thermal comfort decreases prediction accuracy. Nonetheless, the LF_p has been challenged as a reliable index for physical stress assessment. Arai et al. [40] demonstrated that with increasing exercise levels, the subjects' LF_p decreased. Moreover, the LF_p/HF_p has received much criticism for sympathovagal balance assessment [41–44]. Since various evidence has shown that the interactions between the SNS and PNS are rather complex and nonlinear [41,43,45], the LF_p/HF_p, a simple number, which is based on a simple linear interaction between the SNS and PNS, is incapable of accurately measuring the sympathovagal balance [46]. Instead of using the LF_p/HF_p directly, Rosenberg et al. [47] revealed the fact that it is better to use the information in the LF and HF separately by proposing a two-dimensional representation of the LF and HF.

Furthermore, although numerous studies have extensively investigated applying the Fast Fourier Transform (FFT) to calculate the power of the LF and HF, the FFT cannot deal well with artifacts or irregularities in the RRIs, which may be generated by measuring errors or physical activities such as a deep breath as pointed out by Rosenberg et al. [47], resulting in approximate rectangular patterns (the width of which is equal to the applied sliding time window) in the computed plots of the LF_p, HF_p, and LF_p/HF_p over time. To address this challenge, in Rosenberg et al. [47], instead of using the FFT to compute the power of the LF and HF, the authors proposed to use the instantaneous amplitude (iA) of the LF and HF obtained through the HT [48–50].

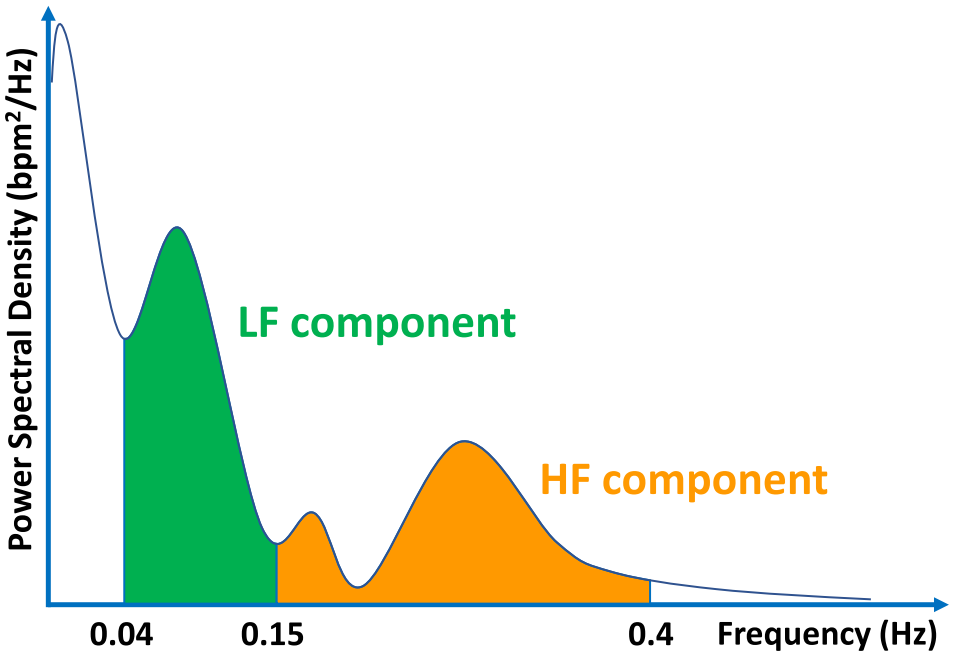

Fig. 2. Schematic of the Low-frequency component (LF) and the High-frequency component (HF) in the Power Spectral Density (PSD) of the IHR.

3. Methodology

In this section, we investigate using HRV indices as features for personal ATS modeling. In order to account for the problems mentioned above, the FFT and HT were both conducted and compared for frequency-domain HRV feature extraction using the subjects' RRIs. In addition, time-domain HRV features were also extracted. Then, we investigate the possibility of enhancing thermal comfort prediction by utilizing HT-based features and other HRV features together by utilizing machine learning techniques. Next, multiple feature sets were defined to evaluate the proposed HRV features. A novel continuous thermal sensation acquisition system is proposed to gather the subjects' approximate continuous thermal sensation. Finally, due to the continuous ATS assumption, machine learning regressions were carried out to evaluate the performance of each feature set in predicting the subjects' personal ATS.

3.1. FFT and HT-based frequency-domain HRV feature extraction

We used the FFT and HT to calculate frequency-domain HRV features, the procedures of which are outlined in Algorithm 1 and Algorithm 2.

For the FFT-based method, firstly, linear interpolation was applied to the RRIs with an interval of 1 s. Second, the instantaneous heart rate (IHR) was calculated by Eq. (1) using the interpolated RRI. Next, a 5-min-long sliding time window with a 1-s increment was used to divide the IHR into overlapping segments. Here, for reliable assessment, we adopted the length of the sliding time window to be 5 min to ensure that the lowest frequency (0.04 Hz) of the lower cut-off of the LF occurs sufficiently (12 cycles in 5 min) in every sliding time window as suggested by [47].

$$\mathrm{IHR} = \frac{60\ \mathrm{s}}{\mathrm{RRI}} \tag{1}$$

Next, the FFT was applied to the IHR to generate the FFT signals for every sliding time window. The FFT is a very fast algorithm for the computation of the Discrete Fourier Transform (DFT) [51,52]. The FFT of a length-N sequence is defined as Eq. (2). In Eq. (2), $x[n]$ is a length-N sequence, $y[k]$ is the FFT of the $x[n]$ with the same length. The FFT calculation was conducted using the Python Scipy package.

$$y[k] = \sum_{n=0}^{N-1} e^{-2\pi j \frac{kn}{N}} x[n] \tag{2}$$

Finally, the power for every sliding time window was calculated using Eq. (3). In Eq. (3), the denominator is the 5-min-long (300 s) time window, and the numerator is the square of the magnitude of the FFT of the IHR. Then, the $\mathrm{LF_p}$ and $\mathrm{HF_p}$ were computed by the integral of the power according to their corresponding frequency bands, i.e., LF: 0.04–0.15 Hz, HF: 0.15–0.4 Hz.

$$\mathrm{PSD} = \frac{|\mathrm{FFT}|^2}{300\ \mathrm{s}} \tag{3}$$

Algorithm 1 Calculation method of the $\mathrm{LF_p}$ and $\mathrm{HF_p}$

Input: RRIs
Output: $\mathrm{LF_p}$ and $\mathrm{HF_p}$
1: Apply linear interpolation to the original RRI with an interval of 1 s
2: Calculate the IHR using the interpolated RRI
3: Divide the IHR using a 5-min-long sliding time window with a 1-s increment
4: Apply the FFT to every sliding time window of the IHR to compute the power and obtain the $\mathrm{LF_p}$ and $\mathrm{HF_p}$ at every corresponding time point

For the HT-based method, first, linear interpolation was applied to the RRIs with an interval of 1 s. Second, the FFT was used to bandpass-filter the RRIs into the LF and HF. Third, the HT was applied to the LF and HF to compute the analytic signals. The analytic signal $x_a(t)$ of signal $x(t)$ is calculated by Eq. (4), where F is the Fourier Transform operator, U is the unit step function. Then, the y at the right side of Eq. (4) is the HT of $x(t)$ [53,54]. The iA is obtained by the magnitude of the analytic signal, as indicated by Eq. (5), where $x_{iA}(t)$ is the iA of $x_a(t)$. The HT calculation was conducted using the Python Scipy package.

$$x_a(t) = F^{-1}(F(x)2U) = x(t) + iy \tag{4}$$

Finally, the LF_{iA} and HF_{iA} at every time point from the complex-valued analytic signals were obtained by Eq. (5).

$$x_{iA}(t) = |x_a(t)| \tag{5}$$

Different from [47], the process of removing the outliers by excluding the 20% largest and smallest values was not carried out in this study to keep consistent with the FFT-based method for comparison.

Algorithm 2 Calculation method of the LF_{iA} and HF_{iA} [47]

Input: RRIs
Output: LF_{iA} and HF_{iA}
1: Apply linear interpolation to the original RRI with an interval of 1 s
2: Use the FFT to bandpass-filter the interpolated RRI into the LF and HF
3: Apply the HT to the LF and HF to compute the analytic signals
4: Obtain the respective iA at every time point from the complex-valued analytic signals of the LF and HF

3.2. Time-domain HRV feature extraction

In addition to the frequency-domain HRV features extracted by the FFT and HT, we also calculated the time-domain HRV indices [9], i.e., the standard deviation of the difference between adjacent RRIs (SDSD), the square root of the mean of the sum of the difference of successive RRIs (RMSSD), the percentage of RRI pairs that differ by 50 ms in the entire recording (pNN_{50}), over a 5-min-long sliding time window with a 1 s increment, as shown in Eqs. (6)–(8). In Eqs. (6)–(8), the RR_i is the ith RRI in successive RRI series. Moreover, in [55], Choi et al. demonstrated that the heart rate itself is relevant for thermal comfort modeling. Therefore, the RRI was also used as a time-domain feature.

$$\mathrm{SDSD} = \sqrt{\frac{\sum_{i=1}^{N}(RR_i - \overline{RR})^2}{N-1}} \tag{6}$$

$$\mathrm{RMSSD} = \sqrt{\frac{1}{N-1}\sum_{i=1}^{N-1}(RR_{i+1} - RR_i)^2} \tag{7}$$

$$\mathrm{pNN_{50}} = \frac{1}{N-1}\sum_{i=1}^{N}(|RR_i - RR_{i+1}| > 50\ \mathrm{ms}) \tag{8}$$

3.3. Correlation analysis

The Pearson correlation coefficients between each subject's HRV features and the personal ATS were calculated, provided that all HRV features were smoothed using the moving average method by Eq. (9) as follows before calculating the correlations. The correlation analysis result is discussed in Section 5.1.

$$\overline{X_t} = \frac{\sum_{i=-150}^{i=149} X_{t+i}}{300} \tag{9}$$

In Eq. (9), X_t is a certain HRV feature at time t; $\overline{X_t}$ is the smoothed HRV feature at time t. The sliding time window was selected as 5 min (300 s) to keep consistent with the sliding time window used in the FFT-based method.

3.4. Multiple HRV feature sets

To analyze and compare the validity and benefits of the extracted FFT, HT, and time-domain features for personal ATS assessment, multiple feature sets were defined as follows. First, the same to the correlation analysis, all the HRV features were smoothed using the moving average method using Eq. (9) before inputting to the regression model. Second, the time-domain features were combined to form the Base feature set (Base). Third, the FFT and HT features were combined separately to form the FFT and HT feature sets (F and H). Finally, seven feature sets were defined in total by different combinations of the Base, FFT, and HT feature sets, as shown below.

- Base feature set (Base):
  consisted of RRI, SDSD, RMSSD, and pNN_{50}
- FFT feature set (F):
  consisted of LF_p, HF_p, and LF_p/HF_p
- HT feature set (H):
  consisted of LF_{iA}, HF_{iA}, and LF_{iA}/HF_{iA}
- Base and FFT feature set (BaseF):
  consisted of Base and FFT feature sets
- Base and HT feature set (BaseH):
  consisted of Base and HT feature sets
- FFT and HT feature set (FH):
  consisted of FFT and HT feature sets
- Base, FFT and HT feature set (BaseFH):
  consisted of Base, FFT, and HT feature sets

3.5. Regression algorithm

Since the HRV indices are continuous values, correspondingly, finer thermal sensations can provide more detailed information to the labels for training the model. From this point of view, it may also be possible to use finer discrete thermal sensations as labels by utilizing classifications. However, the more categories in the classification, the lower the prediction accuracy will be obtained. Theoretically, if we use infinite categories in thermal sensation for classifications, the accuracy will become zero at last. Based on this, it would be better to use continuous thermal sensations as labels and use regression algorithms instead to fundamentally solve this problem.

In order to deal with the non-linear interactions between the SNS and PNS as well as the non-linear representations of the LF_p/HF_p and LF_{iA}/HF_{iA}, we used the MLP regression algorithm to evaluate the validity of each feature set defined in Section 3.4 to predict personal ATS since the MLP algorithm can account for non-linearities. The MLP regression model was trained using the Python Scikit-learn package. Optimal hyper-parameters of the MLP regression model were obtained using the grid search technique for each subject. In the MLP regression model, based on the fact that the hyper-parameter 'hidden_layer_sizes' is usually selected as between half of the input size and twice the input size, the most commonly used hyper-parameter candidates were selected as follows: 'hidden_layer_sizes': [(6,), (8,), (10,), (12,), (14,), (16,) (18,), (20,)], 'max_iter'=200, 'activation': ['tanh', 'relu'], 'solver': ['sgd', 'adam'], 'alpha': [0.0001, 0.05], 'learning_rate': ['constant', 'adaptive']. The mean squared error (MSE) was used as the metric.

The feature sets defined in Section 3.4 were used as the training data after normalization, and the subjects' ATS data were used as labels for personal ATS regressions. Since this study is aimed at personal ATS assessment, the data capacity is not large (2400 data points for each subject). In order to make full use of the data, we carried out a 10-fold blocked cross-validation as suggested by [56,57] without shuffling the data since the data have time dependencies, in which each subject's data samples were segmented into ten equal-sized parts according to time order. Next, by repeating the process of using nine parts as the training set and using the remaining one as the test set, each part will be used once as the test set and produce the corresponding prediction result. By combining the prediction results generated from all test sets, the entire prediction result can be obtained.

3.6. Novel continuous thermal sensation acquisition system

The 7-point Absolute Thermal Sensation Scale (7-point ATSS) proposed in [11], with seven categories "very cold (−3)", "cold (−2)", "cool (−1)", "neutral (0)", "warm (+1)", "hot (+2)", "very hot (+3)" in

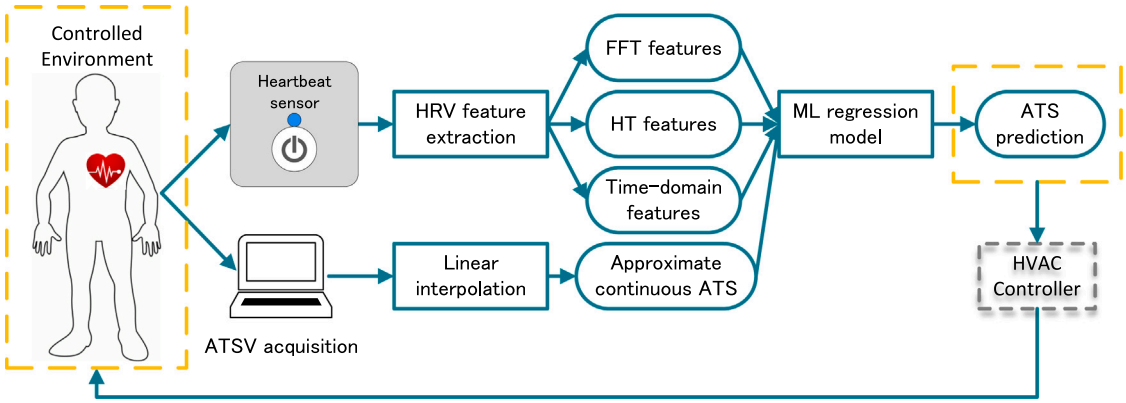

Fig. 3. Overview system architecture of the proposed ATS prediction framework for an occupant-centered HVAC control system.

total, each category in which is called an Absolute Thermal Sensation Vote (ATSV), was utilized by the subjects to gather real-time ATSVs. The "cool", "neutral", "warm" ATSVs are defined to represent comfortable sensations, and the remains represent uncomfortably hot or cold sensations. A laptop computer was used for the subjects' real-time ATSV input. The number keys "1", "2", "3", "4", "5", "6", and "7" represent the ATSVs "very cold (−3)", "cold (−2)", "cool (−1)", "neutral (0)", "warm (+1)", "hot (+2)", "very hot (+3)", respectively.

An alarm clock program was installed on the laptop computer to serve as a reminder for the ATSV input, ringing every 20 s. The subjects were requested to confirm at least once whether the ATS had changed or not when hearing the alarm. If the ATS has changed, the subjects were requested to input the ATSV instantly. As this study considers the ATS as continuous and focuses on real-time thermal comfort assessment under transient thermal environments, it is necessary to obtain as many thermal sensation details as possible. In fact, instead of inputting the ATSV only when an alarm is heard, the subjects were asked to input the ATSV whenever a change in their ATS occurs. The ATSVs were recorded by a small keylogger program written by Python. The timestamps of the recordings of the keyboard buttons have a resolution of 0.001 s.

3.6.1. ATS processing method

For the ATS processing method, the ATS between the experiment start time and the first ATSV timestamp was considered to be the same as the first ATSV; the ATS between the last ATSV timestamp and the experiment end time was considered to be the same as the last ATSV. Since the numerical interval between every two adjacent ATSVs in the 7-point ATSS is the same (i.e., 1), e.g., "hot (+2)" minus "warm (+1)" equals 1, the ATSVs in the 7-point ATSS share a linear relationship and the 7-point ATSS is considered a linear scale. Therefore, linear interpolation was applied to the discrete ATSV data owing to the continuous ATS assumption mentioned in Section 1 to obtain the approximate continuous ATS, with a time interval of 1 s to keep consistent with the time resolution of the HRV features. Based on the above-mentioned procedure, the whole ATS can be obtained.

3.7. Overview system architecture

The overview system architecture of the ATS prediction framework is illustrated in Fig. 3.

4. Experimental setup

We conducted the experiment at the environmental test lab of Tokyo Gas Co., Ltd in winter (Feb 2020), which consists of an external environment and an inner chamber, as illustrated in Fig. 4. The thermal condition of the external environment is adjusted by an HVAC system, which is equipped with a boiler, a chiller, and a humidity controller. On the other hand, an air-conditioner is installed in the inner chamber to heat or cool the inner chamber gradually. We utilized the air-conditioner to create gradual heating and cooling phases in the inner chamber. In addition, the inner chamber has a door equipped to allow heat exchange through the external environment. As the volume of the external environment is much larger than that of the inner chamber, the external environment temperature (T_E) variation can be neglected when opening the door of the inner chamber to make heat exchange, and the inner chamber temperature T_I can be rapidly adjusted to T_E approximately. We utilized this property to create a rapid cooling phase in the inner chamber.

4.1. Thermal conditions

T_E and the relative humidity in the external environment were set to 18 °C and 50% throughout the experiment. Instead of steady-state thermal environments, transient thermal environments were created in this study by various operations of the HVAC system, the air-conditioner, and the door. The door was kept open before the experiment to keep the thermal condition of the inner chamber approximately equal to the thermal condition of the external environment. Two temperature scenarios were created in total, as illustrated in the following Sections.

4.1.1. Scenario I

The upper part of Fig. 5 illustrates the temperature control scheme of Scenario I. First, close the door and turn on the air-conditioner to make a 15-min-long gradual heating phase in the inner chamber with a setpoint of 30 °C. This phase is long enough to make T_I level off during the latter half of the phase by sufficiently heating the inner chamber for 15 min. Second, open the door and turn off the air-conditioner to make a 5-min-long rapid cooling phase. Next, by repeating the first and second phases, a periodic temperature signal with a period of 20 min can be generated. The total duration of Scenario I was 40 min.

4.1.2. Scenario II

The lower part of Fig. 5 illustrates the temperature control scheme of Scenario II. Similar to Scenario I, the first and third phases were identical gradual heating phases by closing the door and turning on the air-conditioner to heat the inner chamber with a setpoint of 30 °C. The second phase is the same as the 5-min-long rapid cooling phases in Scenario I. Different from Scenario I, the last phase in Scenario II was a 15-min-long gradual cooling phase by closing the door and turning on the air-conditioner to cool the inner chamber with a setpoint of 18 °C to keep consistent with the setpoint of the rapid cooling phases (i.e., T_E = 18 °C). The 15-min-long gradual cooling phase was long enough to ensure T_I to be lowered approximately to 18 °C by the end of the cooling phase. In addition, either gradual heating phase in Scenario II was shortened to 10 min to keep the total duration of Scenario II to 40 min to keep consistent with Scenario I.

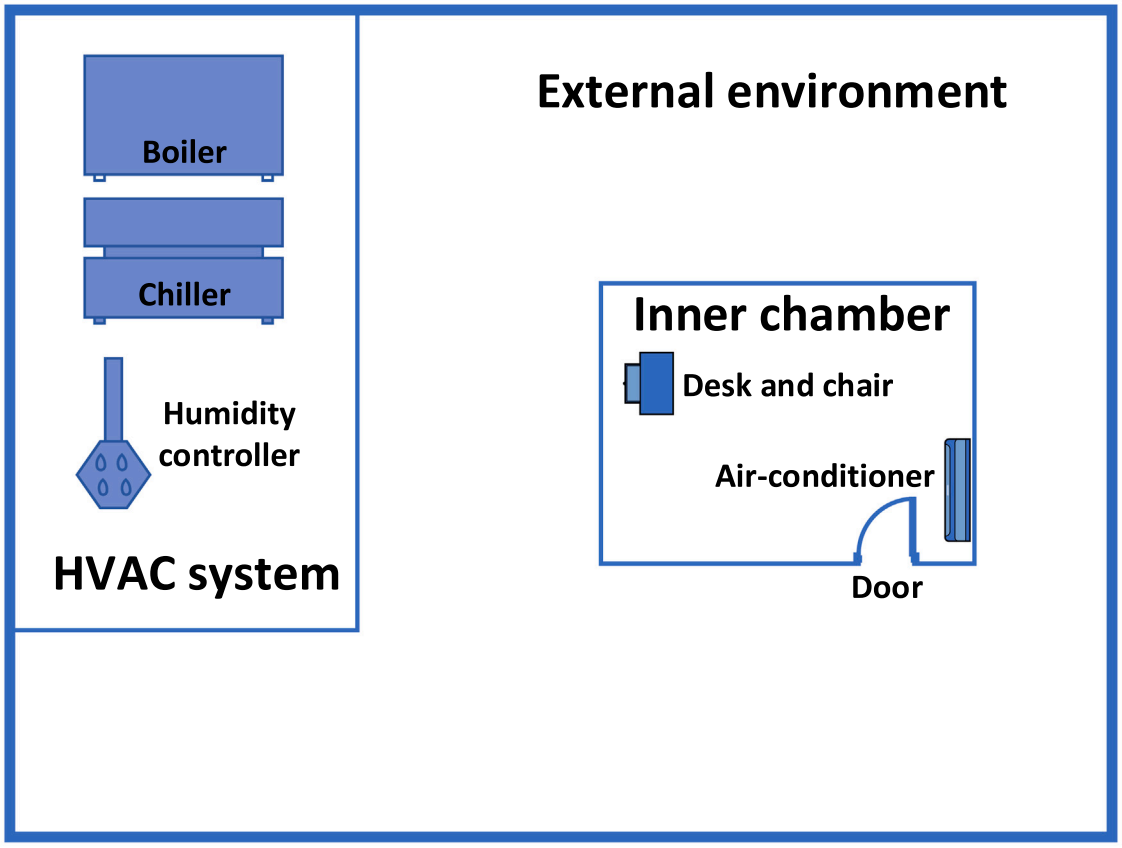

Fig. 4. Schematic of the environmental test lab [11].

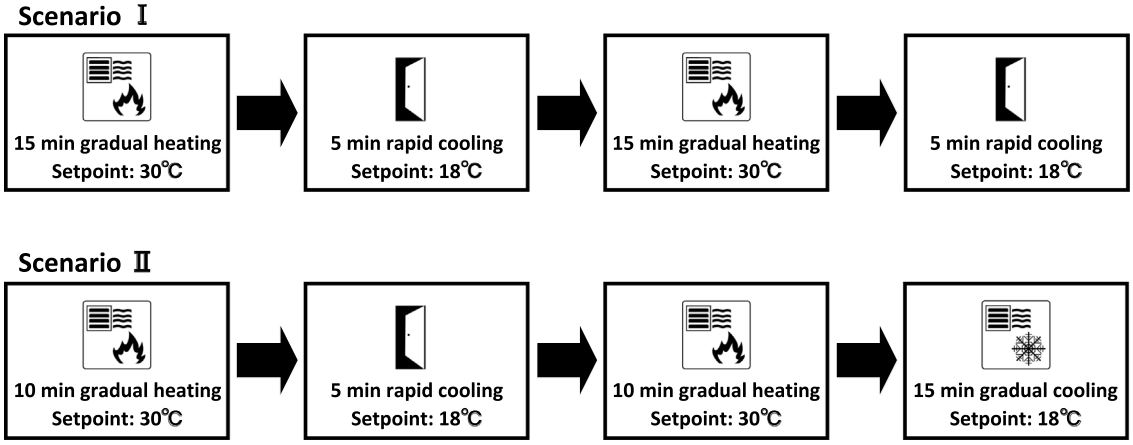

Fig. 5. Two temperature scenarios inside the inner chamber [11].

4.2. Experimental procedure

The specifications of the myBeat WHS-1 are shown in Table 1. The myBeat WHS-1 has a sampling frequency of 1000 Hz. Fig. 6(a–c) shows the front and back of the myBeat WHS-1, and the auxiliary disposable ECG electrode (type: UIR). The back side of the disposable ECG electrode has a viscous layer to keep the disposable ECG electrode sticking on the skin tightly. The myBeat WHS-1 was connected to the disposable ECG electrode and fixed on the subjects' chest to measure the RRIs. After the measurement, the irregularities (i.e., abnormally high or low values) in the original RRIs yielded by the inaccurate measurement of the device were removed manually.

Six subjects participated in the experiment in total. All of them were male students (age: μ: 25.0 years, σ: 1.0 years, weight: μ:72.5 kg, σ: 13.0 kg, height: μ: 177.3 cm, σ: 7.0 cm) at the University of Tokyo. Three students were randomly chosen and dispatched to Scenario I, and the other three were dispatched to Scenario II.

Before the experiment, a desk and a chair were prepared in the inner chamber for the subjects to simulate sedentary office activities. The laptop computer for the subjects' ATSV input was placed on the desk. The desk and chair were placed not to directly confront the airflow from the air-conditioner or the door, as shown in Fig. 4. During the experiment, the subjects were requested to sit down on the chair and press the keyboard buttons to input the ATSV (small range of

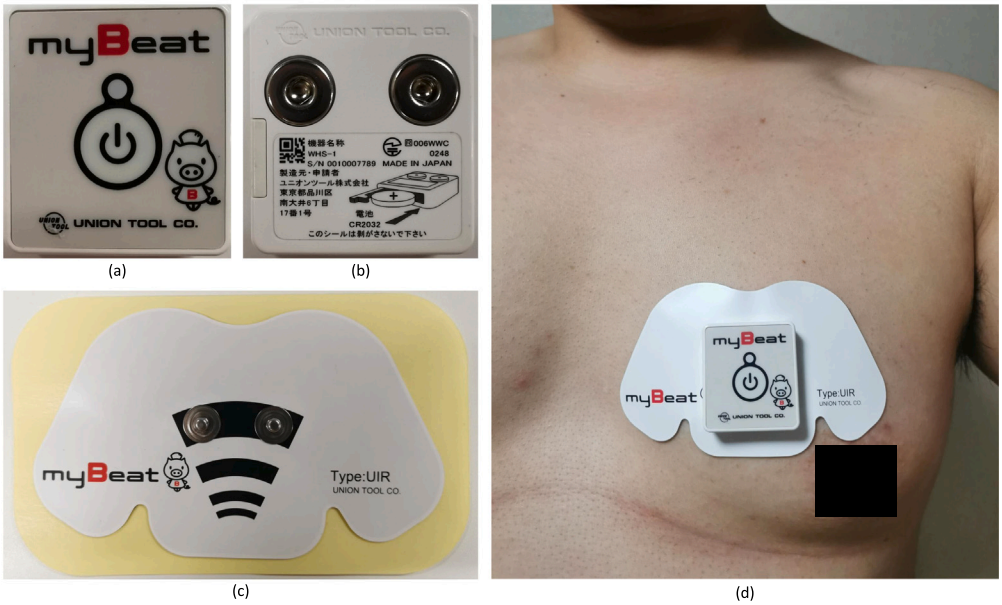

Fig. 6. The heartbeat sensor myBeat WHS-1: (a) front, (b) back, (c) the auxiliary disposable ECG electrode (type: UIR), (d) the mounting state of the myBeat WHS-1 on a male subject's chest.

Table 1
Specifications of the myBeat WHS-1.

Features	Descriptions		
Dimensions	40.8 mm × 37.0 mm × 8.9 mm		
Weight	13 g		
Battery	Coin type lithium-ion battery		
Memory	7-day measurement		
Sampling frequency	1000 Hz		
Price	$394		
Accuracy	Input ECG	60 bpm	120 bpm
	Mean error	−0.0787 ms	−0.0720 ms
	Standard error	1.98 ms	2.08 ms

motions allowed). The subjects were requested to wear the same clothes (black short sleeves, trousers, and cotton socks) provided by us during the experiment. The subjects were requested to put their hands on their thighs when not pressing the keyboard. Furthermore, a thermal insulation pad was placed directly under the desk on the floor for the subjects' feet to prevent unnecessary conductive heat loss through the floor. The subjects were requested to perform hair removal on their chest before the experiment. During the preparation time (20 min), we fixed the myBeat WHS-1 onto the subjects' chest as illustrated in Fig. 6(d). The subjects were required to use the left hand to input the ATSV as the right hand was adhered with thermocouples by medical tapes in order to measure the skin temperatures. The subjects were confirmed whether their current ATS was unchanging or not (whether the RTS is "no change" or not) for preparation before the experiment to maintain a steady-state thermal sensation. Fig. 7 shows a male subject and the mounting state of the experimental devices.

The ambient air temperature was measured by a pair of Type *T* thermocouples (copper-constantan) per s placed 60 cm above the floor near the subject with accurate temporal synchronization and recorded by a data logger (Midi LOGGER GL840: accuracy: ±0.5 °C, resolution: 0.01 °C), as shown in Fig. 7. The subjects were not aware of the opening and closing of the door and the operations of the air-conditioner and were requested to input the ATSV according to subjective thermal feelings. The Research Ethics Committee of the University of Tokyo approved the experiment.

5. Results and discussion

Table 2 summarizes the total duration of each ATS category of each subject by rounding the interpolated ATS to the nearest whole numbers. Significant individual differences can be observed among the subjects as shown in Table 2. In Scenario I, subject 3 only had the "cold", "cool", "neutral", and "warm" ATS throughout the experiment but lacked the "very cold", "hot", or "very hot" ATS. In Scenario II, subjects 4 and 5 had no "very hot" ATS throughout the experiment.

5.1. Correlation analysis result

Table 3 shows the Pearson correlation coefficients between each subject's HRV features and the personal ATS. In Table 3, the absolute values of Pearson correlation coefficients more than 0.30 (more than moderate correlation) are shown in bold font.

As can be observed in Table 3, for either the FFT or HT features, all subjects have 14 features that have moderate or strong linear correlations with the ATS in Scenarios I and II in total. Therefore, it is concluded that both the FFT and HT features can be relevant for thermal comfort modeling.

For the RRI, significant Individual differences can be observed that for subjects 1, 2, 3, and 6, the RRI highly correlates with the ATS, whereas, for subjects 4 and 5, the RRI only shows a weak correlation with the ATS. For the pNN_{50}, significant individual differences can be observed that the pNN_{50} has a correlation with the ATS more than moderate for subjects 1, 4, 5, and 6 but nearly uncorrelated with the ATS for subjects 2 and 3.

Also, it is noteworthy that the HF_p and LF_{iA} show a correlation with the ATS more than moderate for all subjects, indicating that these frequency-domain features are more robust for ATS modeling than the time-domain features.

5.2. Data visualization

Figs. 8 and 9 show the FFT features, HT features, and time-domain features of two subjects from Scenarios I and II after smoothing and normalization, respectively. In Figs. 8 and 9, the thick blue line indicates the air temperature; the black circles indicate the original ATSVs;

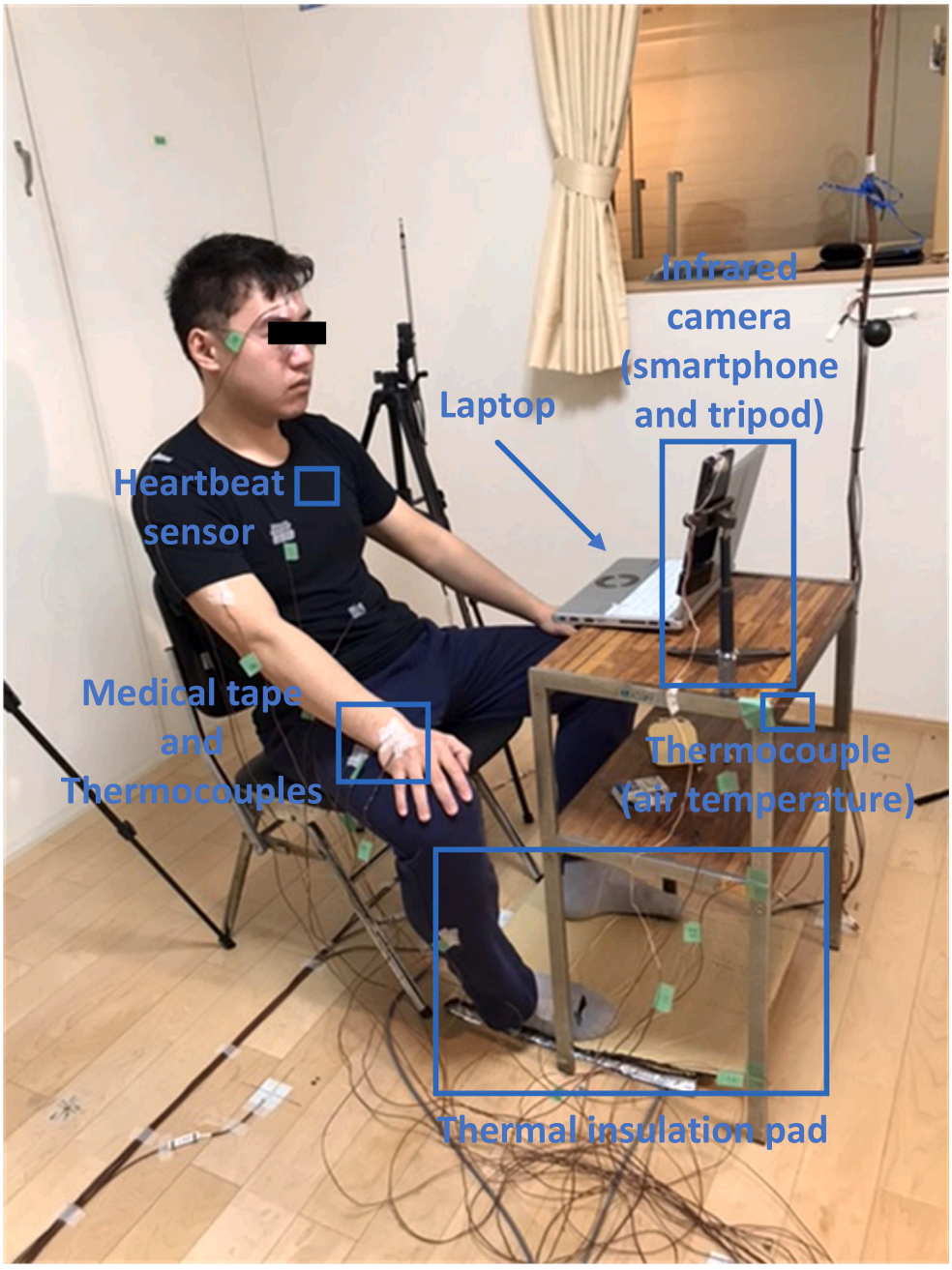

Fig. 7. The mounting state of the experimental devices on a male subject [11].

Table 2
Total duration (s) of each subject's each ATS category.

Scenario	Subject ID	ATS						
		very cold (−3)	cold (−2)	cool (−1)	neutral (0)	warm (+1)	hot (+2)	very hot (+3)
I	1	226	423	183	288	570	464	246
	2	543	277	98	184	599	675	24
	3	NaN	1002	453	658	287	NaN	NaN
II	4	36	747	306	504	525	282	NaN
	5	482	453	145	202	937	181	NaN
	6	43	304	331	447	449	370	456

the green dashed line indicates the interpolated ATS label. In Figs. 8(a, b) and 9(a, b), the light blue lines indicate the LF_p and LF_{iA}; the orange lines indicate the HF_p and HF_{iA}; the green lines indicate the LF_p/HF_p and LF_{iA}/HF_{iA}. In Figs. 8(c) and 9(c), the light blue line indicates the RRI; the orange line indicates the SDSD; the green line indicates the RMSSD; and the red line indicates the pNN_{50}.

In Figs. 8 and 9, many obvious correlations can be observed between the FFT, HT, and time-domain HRV features and the ATS, indicating

Table 3
The Pearson correlation coefficients between personal ATS and HRV features.

HRV feature category		Scenario					
		I			II		
		Subject ID					
		1	2	3	4	5	6
FFT features	LF_p	−0.21	**0.58**	0.21	**−0.57**	**0.31**	**−0.67**
	HF_p	**−0.58**	**−0.72**	**0.45**	**−0.65**	**−0.80**	**−0.67**
	LF_p/HF_p	**0.61**	**0.88**	**−0.40**	−0.25	**0.51**	0.12
HT features	LF_{iA}	**−0.50**	**0.40**	**0.48**	**−0.58**	**0.41**	**−0.61**
	HF_{iA}	**−0.72**	**−0.45**	0.15	**−0.53**	**−0.37**	**−0.61**
	LF_{iA}/HF_{iA}	**0.51**	**0.64**	0.27	0.01	**0.76**	0.05
Time-domain features	RRI	**−0.90**	**−0.90**	**0.68**	0.24	−0.23	**−0.84**
	SDSD	**−0.61**	−0.15	**0.39**	**−0.65**	0.09	**−0.67**
	RMSSD	**−0.73**	**−0.86**	0.21	**−0.76**	**−0.51**	**−0.79**
	pNN_{50}	**−0.70**	−0.04	−0.02	**−0.71**	**−0.54**	**−0.61**

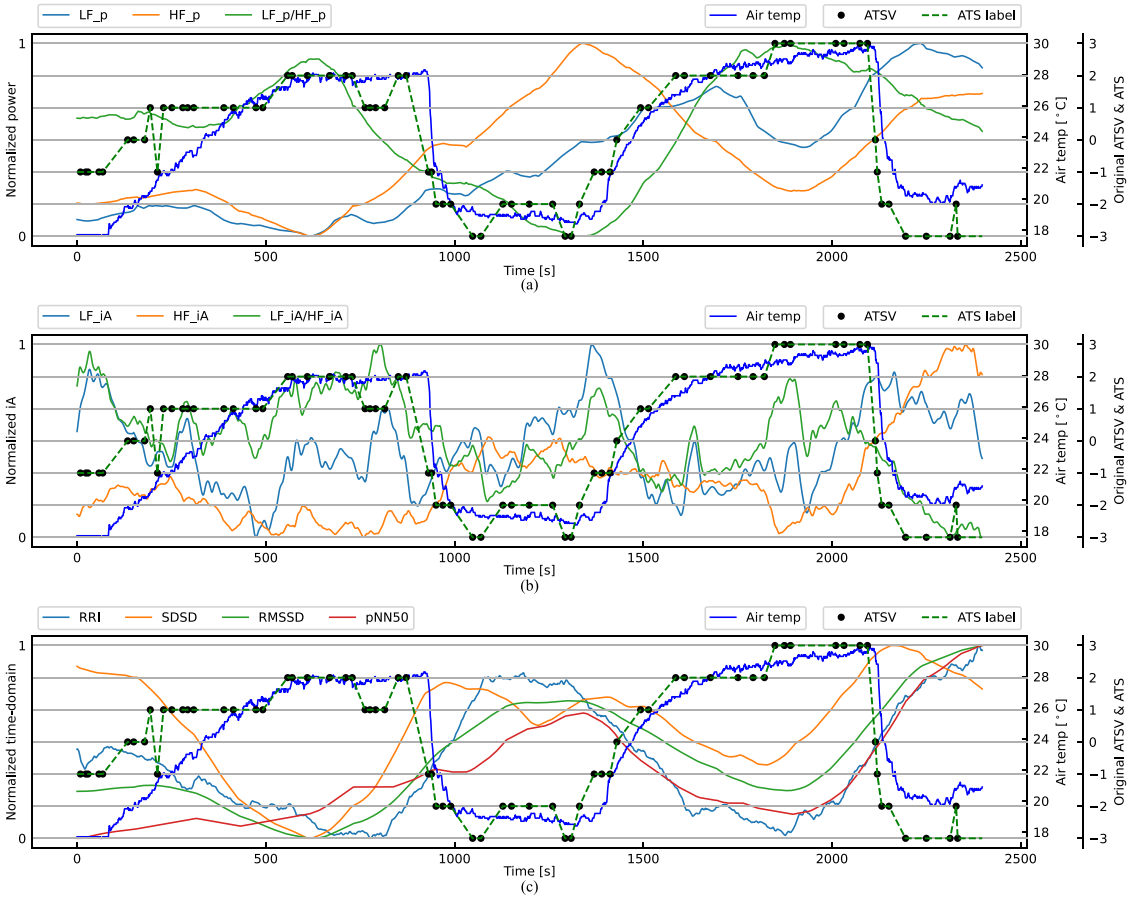

Fig. 8. Air temperature, original ATSVs, ATS label, normalized FFT features (a), HT features (b), and time-domain features (c) (Scenario I & subject 1). (For interpretation of the references to color in this figure legend, the reader is referred to the web version of this article.)

that it is reasonable to use the FFT, HT, and time-domain features for ATS modeling, which agrees with the correlation analysis illustrated in Section 5.1.

5.3. Personal ATS assessment

Table 4 shows the average MSE and coefficient of determination (R^2) of personal ATS predictions using the seven feature sets defined in Section 3.4. As can be observed in Table 4, for both the average MSE and R^2 of all subjects in Scenarios I and II, significant results can be summarized as follows.

1. The BaseF feature set outperformed both the Base and F feature sets.
2. The BaseH feature set outperformed both the Base and H feature sets.
3. The FH feature set outperformed both the F and H feature sets.
4. The BaseFH feature set outperformed all the other feature sets.

Moreover, the BaseFH feature set reached the lowest average MSE of 0.76, 0.09 lower than the second-lowest obtained by the BaseH feature set, and reached the highest average R^2 of 0.73, 0.04 higher than the second-highest obtained by the BaseF and BaseH feature sets. Therefore, it is concluded that the HT is no weaker than the FFT in the frequency-domain HRV feature extraction for ATS modeling, which agrees with [47] and the correlation analysis result mentioned in Section 5.1, and it is feasible to combine the FFT, HT, and time-domain

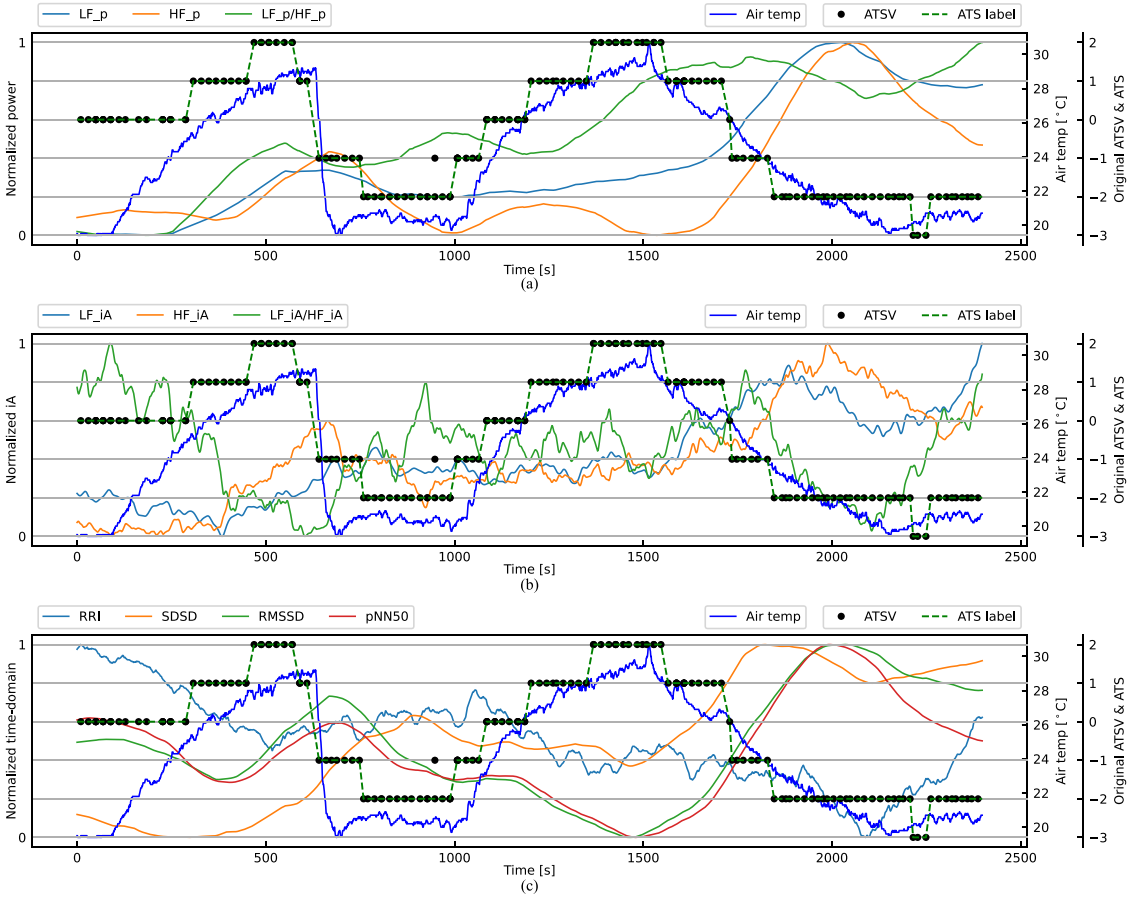

Fig. 9. Air temperature, original ATSVs, ATS label, normalized FFT features (a), HT features (b), and time-domain features (c) (Scenario II & subject 4). (For interpretation of the references to color in this figure legend, the reader is referred to the web version of this article.)

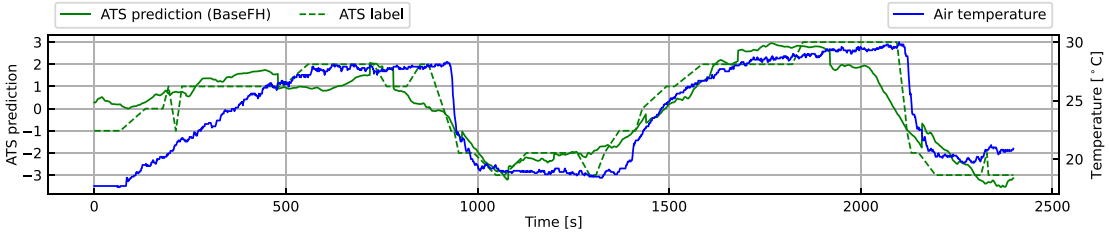

Fig. 10. Personal ATS prediction (BaseFH feature set) (Scenario I & Subject 1).

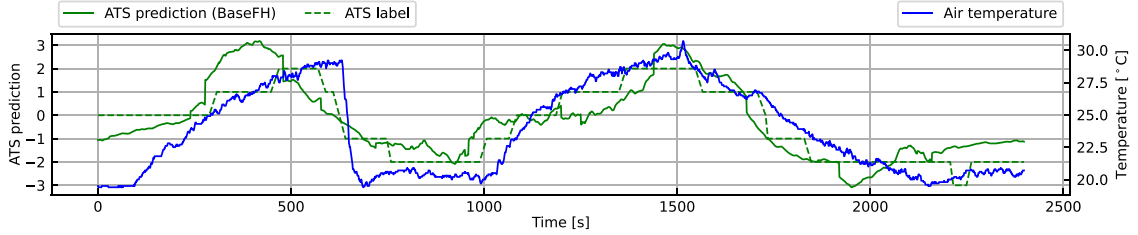

Fig. 11. Personal ATS prediction (BaseFH feature set) (Scenario II & Subject 4).

features together to significantly enhance personal ATS assessment, which could be utilized to build a wearable thermal comfort assessment framework since only one portable and non-intrusive heartbeat sensor is required and contribute to energy conservation in buildings through intelligent HVAC control using the framework.

Figs. 10 and 11 show the ATS predictions using the BaseFH feature set of the two subjects we mentioned before from Scenarios I and II, respectively. In Figs. 10 and 11, the prediction curves generated by the BaseFH feature set track the ATS labels fairly well, indicating the validity of the continuous ATS assumption. As can be observed in

Table 4
Performance metrics of personal ATS predictions in Scenarios I and II for each HRV feature set.

	Scenario	Subject ID	Feature set						
			Base	F	H	BaseF	BaseH	FH	BaseFH
MSE	I	1	0.84	3.97	2.45	0.71	0.96	1.14	0.58
		2	0.65	0.53	3.38	0.52	0.48	0.60	0.41
		3	0.53	1.47	1.15	0.42	0.55	1.42	0.35
		Avg.	0.68	1.99	2.33	0.55	0.66	1.05	0.44
	II	4	0.84	3.97	2.45	0.71	0.96	1.14	0.58
		5	0.65	0.53	3.38	0.52	0.48	0.60	0.41
		6	0.53	1.47	1.15	0.42	0.55	1.42	0.35
		Avg.	1.22	2.00	1.97	1.19	1.05	1.66	1.08
	Avg. (all)		0.95	2.00	2.15	0.87	0.85	1.36	0.76
	Scenario	Subject ID	Feature set						
			Base	F	H	BaseF	BaseH	FH	BaseFH
R^2	I	1	0.79	0.00	0.38	0.82	0.76	0.71	0.85
		2	0.86	0.88	0.26	0.89	0.90	0.87	0.91
		3	0.54	−0.28	0.01	0.64	0.53	−0.23	0.70
		Avg.	0.73	0.20	0.22	0.78	0.73	0.45	0.82
	II	4	0.72	0.18	0.18	0.72	0.77	0.31	0.72
		5	0.60	0.57	0.47	0.62	0.61	0.57	0.65
		6	0.48	0.16	0.28	0.47	0.59	0.38	0.55
		Avg.	0.60	0.30	0.31	0.61	0.66	0.42	0.64
	Avg. (all)		0.66	0.25	0.26	0.69	0.69	0.43	0.73

Figs. 10 and 11, the air temperature during both first rapid cooling phases was no higher than that at the beginning of the experiment. However, in Fig. 10, the subject felt "cool" at the beginning of the experiment but felt "very cold" in the first rapid cooling phase; in Fig. 11, the subject felt "neutral" at the beginning of the experiment but felt "cold" in the rapid cooling phase, indicating the context-dependent property of the ATS, i.e., the ATS is not monotonically determined by the current temperature but can also be influenced by the previous context, and the proposed models track the ATS fluctuations caused by the context-dependent property fairly well in the transient thermal environments, especially in Fig. 10. In Fig. 10, in the first rapid cooling phase, the air temperature abruptly dropped due to the effect of opening the door and continuously decreased with a small slope. However, the subject's ATS got a transition from "very cold" to "cold" during this period. Obviously, our model can even track this transition very well, indicating the validity of the proposed HRV features for personal ATS assessment in the transient thermal environments. As shown in Figs. 10 and 11, since the ATS > +1 denotes uncomfortably hot state, if the period of ATS > +1 could be accurately predicted, it would be better to stop heating the room in advance in order not to run into uncomfortably hot state, not only the occupant's thermal comfort can be assured, but energy can also be saved. The same to the situation of ATS < −1.

5.4. Limitations

This study has some limitations. Firstly, though both the rapid and gradual cooling phases and the gradual heating phase were investigated, the rapid heating phase was not investigated in this study. Secondly, the thermal comfort assessment method for the subjects was investigated in sedentary office activities. The verification in exercise conditions requires further investigation in the future work. Thirdly, though attaching the heartbeat sensor onto the chest is not disturbing, wrist watches could be alternatives for heartbeat measurement in the future work. Finally, as this study is focused on the personalized assessment of thermal comfort and belongs to non-statistical analysis, a relatively small subject sample size (six subjects) was adopted. Even though the results are significant, a larger subject sample size would enhance the validity of the results.

6. Conclusions

In this paper, personal thermal sensation is defined as a continuous function of time, and its validity has been verified. The feasibility of using HRV features for the subjects' personal ATS assessment during sedentary office activities has been verified in transient thermal environments. It has been revealed that it is appropriate to use both the FFT and HT to perform frequency-domain HRV feature extraction for ATS modeling. All of the FFT, HT, and time-domain features have been shown to be relevant for ATS modeling. It has been verified that combining the HT features and other HRV features together can boost personal thermal comfort prediction accuracy. It is feasible to combine the FFT, HT, and time-domain features together to obtain the best ATS prediction. By combining the FFT, HT, and time-domain features together for personal ATS predictions, the average MSE reached the lowest among all seven feature sets. For the ATS prediction using the BaseFH feature set, the average R^2 reached 0.73 in Scenarios I and II. The frequency-domain HRV features HF_p and LF_{iA} show a correlation with the ATS more than moderate for all subjects, indicating that these frequency-domain features show a more robust relevance to the ATS than the time-domain features. Also, the context-dependent property of the ATS has been demonstrated and discussed. The ATS is not monotonically determined by the current temperature but can also be influenced by the previous context. Since the heartbeat measurement only requires a portable and non-intrusive heartbeat sensor, this study facilitates practical applications for wearable thermal comfort assessment frameworks and contributes to energy conservation in buildings.

CRediT authorship contribution statement

Ziyang Wang: Writing – review & editing, Writing – original draft, Methodology, Conceptualization. **Ryuji Matsuhashi:** Supervision, Project administration, Funding acquisition. **Hiroshi Onodera:** Visualization, Software.

Declaration of competing interest

The authors declare that they have no known competing financial interests or personal relationships that could have appeared to influence the work reported in this paper.

Data availability

The authors do not have permission to share data.

Acknowledgments

The authors would like to acknowledge our partners, Aizawa Reina and Yokoyama Chikato from Tokyo Gas Co., Ltd., for their wonderful collaboration, valuable discussions, and suggestions. Without Aizawa-san's precious advice, this paper could not exist. Also, experimental apparatus support from Tokyo Gas Co., Ltd. is acknowledged.

References

[1] Buildings - topics - IEA, 2020, Accessed: 2022-05-20 https://www.iea.org/topics/buildings.
[2] The future of cooling - IEA, 2020, Accessed: 2022-05-20 https://www.iea.org/reports/the-future-of-cooling.
[3] Ashrae, ANSI/ASHRAE Standard 55-2017 : Thermal Environmental Conditions for Human Occupancy, Vol. 2017, ASHRAE Inc., 2017, p. 66.
[4] W. Jung, F. Jazizadeh, Comparative assessment of HVAC control strategies using personal thermal comfort and sensitivity models, Build. Environ. 158 (March) (2019) 104–119.
[5] N. Montano, T.G. Ruscone, A. Porta, F. Lombardi, M. Pagani, A. Malliani, Power spectrum analysis of heart rate variability to assess the changes in sympathovagal balance during graded orthostatic tilt, Circulation 90 (4) (1994) 1826–1831.

[6] M. Bootsma, C.A. Swenne, H.H. Van Bolhuis, P.C. Chang, V.M. Cats, A.V. Bruschke, Heart rate and heart rate variability as indexes of sympathovagal balance, Am. J. Physiol. 266 (4 Pt 2) (1994) H1565–71.

[7] H. Otzenberger, C. Gronfier, C. Simon, A. Charloux, J. Ehrhart, F. Piquard, G. Brandenberger, Dynamic heart rate variability: a tool for exploring sympathovagal balance continuously during sleep in men, Am. J. Physiol. 275 (3) (1998) H946–50.

[8] W. Liu, Z. Lian, Y. Liu, Heart rate variability at different thermal comfort levels, Eur. J. Appl. Physiol. 103 (3) (2008) 361–366.

[9] K.N. Nkurikiyeyezu, Y. Suzuki, G.F. Lopez, Heart rate variability as a predictive biomarker of thermal comfort, J. Ambient Intell. Humaniz. Comput. 9 (5) (2018) 1465–1477.

[10] H. Zhu, H. Wang, Z. Liu, D. Li, G. Kou, C. Li, Experimental study on the human thermal comfort based on the heart rate variability (HRV) analysis under different environments, Sci. Total Environ. 616–617 (2018) 1124–1133.

[11] Z. Wang, H. Onodera, R. Matsuhashi, Proposal of relative thermal sensation: Another dimension of thermal comfort and its investigation, IEEE Access 9 (2021) 36266–36281.

[12] Z. Wang, R. Matsuhashi, H. Onodera, Pilot study on early warning systems for thermal discomfort using body surface temperature for energy conservation in the building sector, 2021, Accessed: 2022-3-21 https://www.energy-proceedings.org/wp-content/uploads/icae2021/1644391188.pdf.

[13] Biosensing standard - myBeat heartbeat sensor, 2021, Accessed: 2022-05-21 https://www.uniontool-mybeat.com/SHOP/101970/284157/list.html.

[14] N. Charkoudian, Skin blood flow in adult human thermoregulation: how it works, when it does not, and why, Mayo Clin. Proc. 78 (5) (2003) 603–612.

[15] D.L. Kellogg Jr., In vivo mechanisms of cutaneous vasodilation and vasoconstriction in humans during thermoregulatory challenges, J. Appl. Physiol. 100 (5) (2006) 1709–1718.

[16] S. Takada, S. Matsumoto, T. Matsushita, Prediction of whole-body thermal sensation in the non-steady state based on skin temperature, Build. Environ. 68 (2013) 123–133.

[17] A. Ghahramani, G. Castro, S.A. Karvigh, B. Becerik-Gerber, Towards unsupervised learning of thermal comfort using infrared thermography, Appl. Energy 211 (October 2017) (2018) 41–49.

[18] Y. Yao, Z. Lian, W. Liu, C. Jiang, Y. Liu, H. Lu, Heart rate variation and electroencephalograph - The potential physiological factors for thermal comfort study, Indoor Air 19 (2) (2009) 93–101.

[19] S. Yang, M.P. Wan, W. Chen, B.F. Ng, S. Dubey, Model predictive control with adaptive machine-learning-based model for building energy efficiency and comfort optimization, Appl. Energy 271 (2020) 115147.

[20] E. Schmidt, R. Decke, R. Rasshofer, A.C. Bullinger, Psychophysiological responses to short-term cooling during a simulated monotonous driving task, Appl. Ergon. 62 (2017) 9–18.

[21] E. Schmidt, A.C. Bullinger, Mitigating passive fatigue during monotonous drives with thermal stimuli: Insights into the effect of different stimulation durations, Accid. Anal. Prev. 126 (vember 2017) (2019) 115–121.

[22] J.C.F. Siqueira, L.B. da Silva, A.S. Coutinho, R.M. Rodrigues, Analysis of air temperature changes on blood pressure and heart rate and performance of undergraduate students, Work 57 (1) (2017) 43–54.

[23] J.I. Halonen, A. Zanobetti, D. Sparrow, P.S. Vokonas, J. Schwartz, Relationship between outdoor temperature and blood pressure, Occup. Environ. Med. 68 (4) (2011) 296–301.

[24] B.R.M. Kingma, A.J.H. Frijns, W.H.M. Saris, A.A. van Steenhoven, W.D.v.M. Lichtenbelt, Increased systolic blood pressure after mild cold and rewarming: relation to cold-induced thermogenesis and age, Acta Physiol. 203 (4) (2011) 419–427.

[25] S.I.-U.-H. Gilani, M.H. Khan, M. Ali, Revisiting fanger's thermal comfort model using mean blood pressure as a bio-marker: An experimental investigation, Appl. Therm. Eng. 109 (2016) 35–43.

[26] X. Su, Z. Wang, Y. Xu, N. Liu, Thermal comfort under asymmetric cold radiant environment at different exposure distances, Build. Environ. 178 (2020) 106961.

[27] S. Akselrod, D. Gordon, F.A. Ubel, D.C. Shannon, A.C. Berger, R.J. Cohen, Power spectrum analysis of heart rate fluctuation: a quantitative probe of beat-to-beat cardiovascular control, Science 213 (4504) (1981) 220–222.

[28] M. Pagani, F. Lombardi, S. Guzzetti, G. Sandrone, O. Rimoldi, G. Malfatto, S. Cerutti, A. Malliani, Power spectral density of heart rate variability as an index of sympatho-vagal interaction in normal and hypertensive subjects, J. Hypertens. Suppl. 2 (3) (1984) S383–5.

[29] M. Pagani, F. Lombardi, S. Guzzetti, O. Rimoldi, R. Furlan, P. Pizzinelli, G. Sandrone, G. Malfatto, S. Dell'Orto, E. Piccaluga, Power spectral analysis of heart rate and arterial pressure variabilities as a marker of sympatho-vagal interaction in man and conscious dog, Circ. Res. 59 (2) (1986) 178–193.

[30] Z. Ori, G. Monir, J. Weiss, X. Sayhouni, D.H. Singer, Heart rate variability. Frequency domain analysis, Cardiol. Clin. 10 (3) (1992) 499–537.

[31] N. Montano, A. Porta, C. Cogliati, G. Costantino, E. Tobaldini, K.R. Casali, F. Iellamo, Heart rate variability explored in the frequency domain: a tool to investigate the link between heart and behavior, Neurosci. Biobehav. Rev. 33 (2) (2009) 71–80.

[32] K.C. Bilchick, R.D. Berger, Heart rate variability, J. Cardiovasc. Electrophysiol. 17 (6) (2006) 691–694.

[33] Task Force of the European Society of Cardiology the North A Electrophysiology, Heart rate variability. Standards of measurement, physiological interpretation, and clinical use, Circulation 93 (5) (1996) 1043–1065.

[34] A. Malliani, M. Pagani, F. Lombardi, S. Cerutti, Cardiovascular neural regulation explored in the frequency domain, Circulation 84 (2) (1991) 482–492.

[35] P.K. Stein, M.S. Bosner, R.E. Kleiger, B.M. Conger, Heart rate variability: a measure of cardiac autonomic tone, Am. Heart J. 127 (5) (1994) 1376–1381.

[36] Y. Yao, Z. Lian, W. Liu, Q. Shen, Experimental study on physiological responses and thermal comfort under various ambient temperatures, Physiol. Behav. 93 (1–2) (2008) 310–321.

[37] N. Morresi, S. Casaccia, M. Sorcinelli, et al., Sensing physiological and environmental quantities to measure human thermal comfort through Machine learning techniques, IEEE Sens. J. (2021).

[38] N. Morresi, S. Casaccia, M. Arnesano, G.M. Revel, Impact of the measurement uncertainty on the monitoring of thermal comfort through AI predictive algorithms, Acta Imeko 10 (4) (2021) 221.

[39] Pigliautile, Casaccia, Morresi, Arnesano, et al., Assessing occupants' personal attributes in relation to human perception of environmental comfort: Measurement procedure and data analysis, Build. Constr. News (2020).

[40] Y. Arai, J.P. Saul, P. Albrecht, L.H. Hartley, L.S. Lilly, R.J. Cohen, W.S. Colucci, Modulation of cardiac autonomic activity during and immediately after exercise, Am. J. Physiol. 256 (1 Pt 2) (1989) H132–41.

[41] G.E. Billman, Heart rate variability - a historical perspective, Front. Physiol. 2 (2011) 86.

[42] M.S. Houle, G.E. Billman, Low-frequency component of the heart rate variability spectrum: a poor marker of sympathetic activity, Am. J. Physiol. 276 (1) (1999) H215–23.

[43] D.L. Eckberg, Sympathovagal balance: a critical appraisal. Reply, Circulation 98 (23) (1998) 2643–2644.

[44] B.A. Kingwell, J.M. Thompson, D.M. Kaye, G.A. McPherson, G.L. Jennings, M.D. Esler, Heart rate spectral analysis, cardiac norepinephrine spillover, and muscle sympathetic nerve activity during human sympathetic nervous activation and failure, Circulation 90 (1) (1994) 234–240.

[45] G.E. Billman, Cardiac autonomic neural remodeling and susceptibility to sudden cardiac death: effect of endurance exercise training, Am. J. Physiol. Heart Circ. Physiol. 297 (4) (2009) H1171–93.

[46] G.E. Billman, The LF/HF ratio does not accurately measure cardiac sympatho-vagal balance, Front. Physiol. 4 FEB (February) (2013) 1–5.

[47] W. von Rosenberg, T. Chanwimalueang, T. Adjei, U. Jaffer, V. Goverdovsky, D.P. Mandic, Resolving ambiguities in the LF/HF ratio: LF-hf scatter plots for the categorization of mental and physical stress from HRV, Front. Physiol. 8 (JUN) (2017) 1–12.

[48] D.P. Mandic, N.u. Rehman, Z. Wu, N.E. Huang, Empirical mode decomposition-based time-frequency analysis of multivariate signals: The power of adaptive data analysis, IEEE Signal Process. Mag. 30 (6) (2013) 74–86.

[49] D. Looney, A. Hemakom, D.P. Mandic, Intrinsic multi-scale analysis: a multivariate empirical mode decomposition framework, Proc. Math. Phys. Eng. Sci. 471 (2173) (2015) 20140709.

[50] D. Looney, L. Li, T.M. Rutkowski, D.P. Mandic, A. Cichocki, Ocular artifacts removal from EEG using EMD, in: Advances in Cognitive Neurodynamics ICCN 2007, Springer Netherlands, 2008, pp. 831–835.

[51] T.K. Boehme, R. Bracewell, The Fourier transform and its applications, Am. Math. Mon. 73 (6) (1966) 685.

[52] H.J. Nussbaumer, The fast Fourier transform, in: H.J. Nussbaumer (Ed.), Fast Fourier Transform and Convolution Algorithms, Springer Berlin Heidelberg, Berlin, Heidelberg, 1981, pp. 80–111.

[53] A.V. Oppenheim, Discrete-Time Signal Processing, Pearson Education India, 1999.

[54] L. Debnath, Wavelets and Signal Processing, Springer Science & Business Media, 2012.

[55] J.H. Choi, V. Loftness, D.W. Lee, Investigation of the possibility of the use of heart rate as a human factor for thermal sensation models, Build. Environ. 50 (2012) 165–175.

[56] C. Bergmeir, J.M. Benítez, On the use of cross-validation for time series predictor evaluation, Inform. Sci. 191 (2012) 192–213.

[57] J. Wainer, G. Cawley, Nested cross-validation when selecting classifiers is overzealous for most practical applications, Expert Syst. Appl. 182 (2021) 115222.